AIAA JOURNAL
Vol. 37, No. 4, April 1999

Blunt-Body Wave Drag Reduction Using Focused Energy Deposition

David Riggins,* H. F. Nelson,† and Eric Johnson‡
University of Missouri–Rolla, Rolla, Missouri 65409-0050

A parametric computational study of energy deposition upstream of generic two-dimensional and axisymmetric blunt bodies at Mach numbers of 6.5 and 10 is performed utilizing a full Navier–Stokes computational fluid dynamics code. The energy deposition modifies the upstream shock structure and results in large wave drag reduction and very high power effectiveness. Specifically, drag is reduced to values as low as 30% of baseline drag (no energy deposited into flow) and power effectiveness ratios (ratio of thrust power saved to power deposited into the flow) of up to 33 are obtained. The fluid dynamic and thermodynamic bases of the observed drag reduction are examined.

Nomenclature

D_{mod} = drag of body with energy deposition, two dimensional, N/m; axisymmetrical, N
D_{ref} = drag of body (no energy deposition), two dimensional, N/m; axisymmetrical, N
h = body diameter, body width, 0.015 m
M_∞ = freestream Mach number
$\dot{Q}$ = energy deposition rate, W; two dimensional, kW/m; axisymmetrical, W
R = $D_{\text{mod}}/D_{\text{ref}}$
S = power effectiveness; see Eq. (2)
V_∞ = freestream velocity, m/s
x = distance upstream of body nose to energy deposition point, m

I. Introduction

THE fundamental issue regarding development of hypersonic vehicles is achievement of a sufficient ratio of engine thrust to external drag to ensure adequate cruise and acceleration to perform a designated mission. This ratio must be maintained subject to design constraints, such as limits on thermal heating and/or cooling capacity, structural integrity, etc. Current technology and design techniques are, at best, only marginally adequate for the design of vehicles requiring sustained hypersonic flight in the atmosphere (Mach numbers greater than six). This paper describes a parametric examination of a concept that could result in very large drag reduction and significant relaxation of supersonic and hypersonic vehicle shape requirements. The concept involves modification of the external flowfield to greatly reduce wave drag; this is proposed to be accomplished by utilizing focused energy deposition into the flow by electromagnetic or other means (lasers, microwaves, etc.).

The overall objective is to assess the feasibility of utilizing focused energy deposition for the modification and attenuation of shock wave patterns around blunt bodies in high-speed flow from a fluid/thermodynamic standpoint. A secondary objective is to provide a contrast to proposed drag reduction techniques and related current investigations that specifically involve the upstream ionization of the flow. Significant reductions of external hypersonic vehicle drag for modest onboard power requirements, however obtained, should result in 1) considerably smaller propulsion system requirements, 2) reduced fuel consumption, 3) substantial improvements in structural integrity, 4) smaller system demands, and 5) considerably larger payloads at smaller take-off gross weight. Mission scenarios that may benefit from substantial drag reduction include (but are not limited to) 1) sustained-cruise supersonic and hypersonic transports, 2) military missiles, and 3) single-stage-to-orbit and transatmospheric combined cycle concepts.

It is well known that significant drag reduction for a blunt-nosed body flying at supersonic Mach numbers is obtained using a spike extending forward from the blunt-body nose.[1] For an axisymmetric body, the spike generates a conical oblique shock wave, which encompasses the body and turns the flow upstream of the body. Pressure drag on the body can drop 50% or more because the detached normal shock associated with a blunt body is no longer present. However, the usefulness of the spike is limited due to cooling requirements (viscous heating of the spike results in unacceptably high thermal stresses) and frictional drag occurring on the spike structure. The basic premise of this work is that nonstructural energy spikes (utilizing focused energy deposition) may be able to generate drag reduction similar to or greater than that obtained by either structural spikes or by specifically ionizing the upstream fluid.

For blunt bodies in supersonic and hypersonic flight, there is a historical engineering tradeoff between 1) desirable thermal protection characteristics (as well as the possible realization of high vehicle volumetric efficiencies) and 2) the very high wave drag associated with shock wave formation on such bodies. The usual tendency for supersonic vehicles has been to forego the use of blunt bodies due to the overriding drag issue and employ vehicles with high fineness ratio shapes, i.e., with very long slender fuselages, to reduce wave drag. However, a number of issues arise for slender bodies, including cooling requirements (creating materials and system problems), structural flexing (a major problem with the High-Speed Civil Transport), and high frictional drag. Note that the energy-deposition technique studied in this investigation essentially increases the effective fineness ratio (rather than the structural fineness ratio) of the vehicle, hence allowing for the possibility of lower wave drag, higher volumetric efficiency, reduced thermal loads, reduced propulsion system requirements, and reduced skin friction.

The potential of energy-assisted shaping of high-speed flows has been the subject of a number of earlier investigations. Bushnell[2] has suggested that the concept could provide two benefits: 1) high effective fineness ratio for high-speed vehicles with attendant drag decrease and 2) sonic boom attenuation for supersonic aircraft. Work has previously been done on acoustic attenuation by Miller and Carlson[3,4] and Batdorf.[5] The possibility of obtaining drag reduction using energy sources upstream of blunt bodies has been pioneered in this decade by Myrabo and others; a recent example of their work is an experimental study using a protruding physical spike with a plasma torch.[6] A significant amount of analytical,

Received April 10, 1998; revision received Oct. 12, 1998; accepted for publication Dec. 21, 1998.

*Associate Professor, Department of Mechanical and Aerospace Engineering and Engineering Mechanics. Senior Member AIAA.
†Professor, Department of Mechanical and Aerospace Engineering and Engineering Mechanics. Associate Fellow AIAA.
‡Graduate Research Assistant, Department of Mechanical and Aerospace Engineering and Engineering Mechanics. Student Member AIAA.

experimental, and numerical work on the subject of using energy to modify flowfields has been done in Russia by a number of investigators over the past decade; this work was summarized and reported on in April 1998 at the AIAA 2nd Weakly Ionized Gases Workshop in Norfolk, Virginia. Recently, a computational study of the sonic boom attenuation potential of energy addition was performed using an Euler computational fluid dynamics code (without viscosity or thermal conductivity).[7] However, the current investigation suggests that only (full) Navier–Stokes models can correctly characterize the effects of localized upstream energization of the flow around a blunt body at high speeds.

Russian, European, and American investigators have proposed to accomplish drag reduction for both subsonic and supersonic vehicles by ionization of the upstream flow via plasma-generation methods.[8] At this time, the specific effects of ionization on the flowfield are being actively investigated by a number of researchers. However, the results presented here indicate that larger drag reduction than that currently reported by the large-scale flow ionization work can be achieved through tightly focused, small-scale energy deposition. The ratio of thrust power saved to power necessary to produce the advantageous effect will be shown to be as large as 33:1 for the energy-deposition method; this ratio is far greater than any reported result of upstream ionization. Also, the physics of the drag reduction mechanism reported on in this work is complicated but nevertheless is a purely thermofluid dynamic effect.[9]

The second section of this paper discusses the computational fluid dynamic tools, methodologies, and strategies used. The third section provides a qualitative comparison of the flowfields generated by 1) energy deposition and 2) a physical spike forward of a blunt body in high-speed flow. The fourth section develops performance parameters for characterization of the drag reduction and power effectiveness (in terms of thrust power saved relative to the onboard power necessary to generate the energy). The matrix of specific cases analyzed and their performance parameters are presented in the fifth section. Analysis of the results and discussion concerning the particulars of the drag reduction mechanisms associated with focused energy deposition follow in the sixth section. The seventh and final section of the paper provides a brief summary of the results and makes recommendations regarding this topic.

II. Computational Methodology

The computational fluid dynamics codes that are used are modified versions of the time-marching, finite difference, full Navier–Stokes SPARK code originally developed by Drummond et al.[10] at NASA Langley Research Center in the late 1980s and early 1990s. SPARK was developed primarily for use in high-speed internal mixing and reacting flows. The full viscous Navier–Stokes equations with variable thermodynamic and diffusion quantities and specific heats are solved in an explicit time-marching fashion. Although the capability for modeling injection and reaction exists in the code, this capability has been turned off for all cases analyzed here. Air disassociation is not considered. The accurate time-marching capability of SPARK was particularly desired in the early phase of this investigation due to concerns about possible temporal instability of energy-modified flowfields. This concern was not justified because subsequent calculations have shown high temporal stability of all energy-deposition cases. Both two-dimensional and axisymmetric versions of SPARK are used in this investigation.

The solutions presented have been obtained using a baseline 105 (axial) × 101 (vertical) grid. Embedded boundaries are utilized to describe the blunt-body surface. This grid is extended parametrically for the portion of the study investigating changing the axial location of the energized region; the grid in the axial direction is varied from 105 up to as many as 301 grid points. A representative case was studied with a refined mesh (number of nodes doubled in both directions) to determine the degree of grid convergence. Results for this case are presented in the Appendix. There was no significant change in calculated wave drag or in observed flowfield contours for the solution obtained on this refined grid when compared with the flowfield obtained using the production grid. This study does not attempt to resolve details of the boundary layer on the blunt body. Hence, only wave drag is presented. Viscous drag and heat transfer are not considered. Another baseline case with (additional) upstream grid was examined to determine whether the energy deposition would induce interactions upstream of the energized region itself. This case demonstrated that, at least for the energy levels examined, there were no effects upstream of the energy deposition region due to the energy deposition.

Fixed supersonic inflow conditions corresponding to a standard altitude of 30 km are used on the inflow boundary; simple extrapolation is used on the outflow boundary. Viscous (no-slip) boundary conditions are applied on the surface of the blunt body, with pressure everywhere extrapolated along the local normal to the body surface. The body is treated as adiabatic, i.e., the temperature on the body surface is extrapolated from the interior with the exception that a maximum wall temperature of 2000 K is imposed on the body surface. This limiting temperature has little effect except in the Mach 10 cases. The stagnation streamtube (body centerline) upstream of the body (including the energy-deposition region) is treated as a reflection boundary, i.e., the flow is taken as symmetric about the body centerline axis.

In this study, to model energy deposition into the flow, the energy equation in SPARK was appropriately modified to include a volumetric-based source term. For example, for the two-dimensional cases, this source term effectively represents a cell volumetric heating rate defined as $\dot{Q}/(\Delta V_{ijk} \cdot N_{\text{cell}})$, where ΔV_{ijk} is the volume of the targeted cell lying within the energized region and N_{cell} is the total number of targeted cells within that region. The targeted cell volumes include the full volumes of cells that are directly centered on the bottom boundary in the energized region. The energy deposition effectively represents a direct transfer of energy to the thermal (translational) mode of the gas within the energized volume. The flowfield undergoes a relatively short transient (nonequilibrium) adjustment until conduction, convection, and production of energy are equilibrated and the local associated fluid dynamics become steady. The typical energy-deposition region is rectangular in shape with an (axial) length of about $\frac{1}{15}$ blunt-body diameters and a height of about $\frac{1}{56}$ blunt-body diameters; i.e., the energy input into the flow is tightly focused relative to the body. For all cases discussed, the energy is deposited upstream of the blunt body on the body centerline axis.

Convergence of the flowfield is determined by monitoring drag of the body (the parameter of interest in this study); typically, the drag reaches its asymptotic limit before 20,000 time iterations. However, the solutions are generally run 40,000 iterations to ensure convergence. A time-convergence study for a representative case is discussed in the Appendix. Each energy-deposition case is initialized with the flowfield corresponding to the appropriate baseline (no-energy) blunt-body flow.

All calculations are made assuming laminar flow with a Prandtl number of 0.7. No attempt is made to model the base of the blunt body; for drag calculation purposes, the base of the body may be thought of as the aft end of an impulse engine providing the required thrust at the given cruise condition. The blunt body (depending on specific cases) approximates either a standard missile-body cylinder (for the axisymmetric calculations) with a hemispherical nose or a two-dimensional wing slab with a cylindrical (two-dimensional) nose (for the two-dimensional calculations). The blunt body is at zero angle of attack for all cases.

III. Comparison Between Physical Spike and Focused Energy Deposition

As discussed in the Introduction, the use of a spike upstream of a blunt body can induce large drag reduction. The drag reduction is caused by the relatively small flow disturbance at the tip of the spike, which couples with the downstream blunt body to produce a wedge-shaped, low-velocity region extending from the spike leading edge to the outer contour of the blunt body. Pressures on the face of the blunt body drop dramatically. It is possible to observe the same effect by computationally flying a very small wedge (corresponding to the tip of a spike) upstream of the blunt body. Figures 1a and 1b show pressure contours and velocity vectors obtained for such a case in which a cylindrical-nosed, two-dimensional slab is flown at Mach 6.5 at an altitude of 30 km. It can be seen from Fig. 1 that a very small disturbance, in this case caused by a physical wedge, has a large effect on flowfield structure not only in front of but also

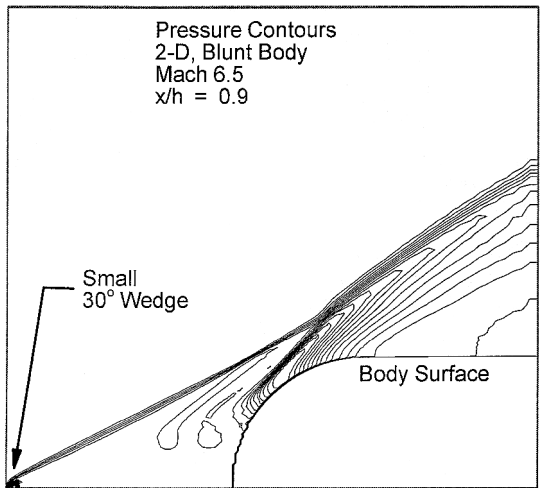

a) Pressure contours

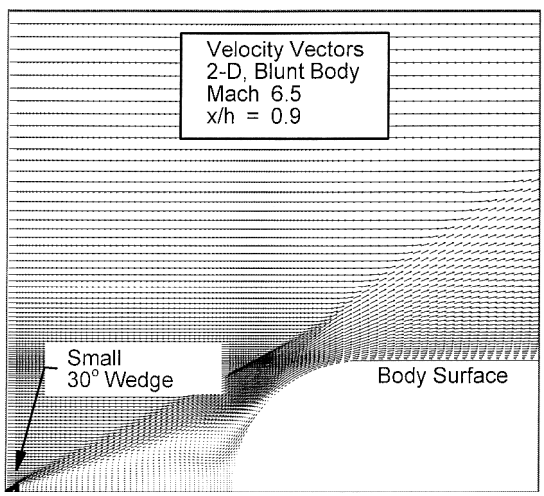

b) Velocity contours

Fig. 1 Flowfield characteristics for two-dimensional blunt body; upstream wedge at $x/h = 0.9$.

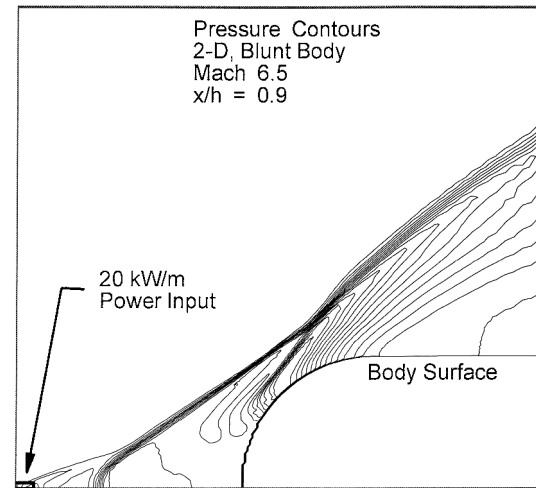

a) Pressure contours

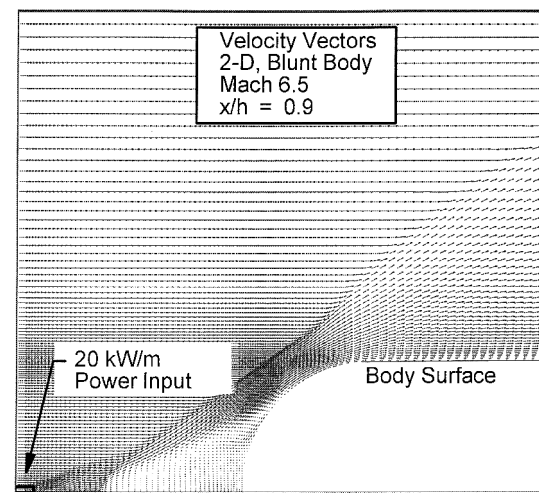

b) Velocity contours

Fig. 2 Flowfield characteristics for blunt body; upstream energization at $x/h = 0.9$.

around the blunt body. It is postulated that energy deposition at the centerline of the upstream flow (tightly focused within a relatively small volume) may produce similar flow characteristics around the blunt body.

Figures 2a and 2b show the pressure contours and the velocity vectors obtained for the same blunt body (without the upstream wedge) with a small amount of highly focused energy addition. There is a striking similarity between the flowfields in Figs. 1 and 2, although the flowfield in Fig. 1 is a result of a structural spike, whereas the flow in Fig. 2 is the result of focused (nonstructural) energy deposition into the flow. The latter method incurs no spike cooling penalty (heating loads are developed on a slender spike), no frictional drag loss, and the intriguing possibility of dynamic control of the flowfield for both drag reduction and vehicle control (reducing or eliminating the need for control surfaces). However, a major disadvantage of the energy-deposition method is the need for an onboard energy generation and focusing system along with associated system weight and volume issues.

IV. Performance Parameters for Energy-Based Drag Reduction

The feasibility of utilizing nonstructural techniques for flowfield modification must be investigated on several levels. Criteria for evaluation must include actual (raw) drag with energy deposition measured against the drag of the baseline blunt body, thrust-power savings for the vehicle made possible by the energy deposition, and onboard power requirements necessary to generate the required energy for the energy deposition. A full parametric evaluation of spatial orientation, location, and magnitude of the focused energy is necessary to fully characterize (and ultimately optimize) the resulting flow structure to maximize the drag reduction and the effectiveness of the energy deposited. Two parameters can be defined that provide insight into the usefulness of the energy-deposition concept. The first parameter,

$$R = \frac{D_{\text{mod}}}{D_{\text{ref}}} = \frac{D_{\text{mod}} V_\infty}{D_{\text{ref}} V_\infty} \tag{1}$$

is the actual drag obtained with the flowfield modification divided by the drag of the body without any flowfield modification (the reference case). Note that R is also equal to the total power required for cruise with the flowfield modification at V_∞ divided by the total power required for cruise with no flowfield modification at V_∞. A second parameter is the power effectiveness S, where

$$S = \frac{(D_{\text{ref}} - D_{\text{mod}}) \cdot V_\infty}{\dot{Q}} = \frac{D_{\text{ref}} V_\infty}{\dot{Q}}(1 - R) \tag{2}$$

S is the ratio of the propulsive power savings due to flowfield modification divided by the power required to modify the flow, or the energy deposition rate. S is the measure of the efficiency of the energy-deposition process from a propulsive/energy management standpoint. Small values of R and large values of S are desirable for drag reduction and effective energy use, respectively.

V. Matrix of Cases Modeled

A large number of cases are examined in this investigation utilizing both two-dimensional and axisymmetric versions of the Navier–Stokes code. Table 1 provides a comprehensive listing and description of 19 representative cases along with performance values R and S. In all cases with energy deposition, the energy is deposited in a very small rectangular region on the stagnation streamline

Table 1 Matrix of cases analyzed and performance results

Case/Mach number	$\dot{Q}$	R	S	x/h
Two dimensional/	0 (Baseline)	1.0	——	——
Mach 6.5	2 kW/m	0.853	45.5	0.9
	10 kW/m	0.591	25.6	0.9
	20 kW/m	0.532	14.5	0.9
	30 kW/m	0.498	10.4	0.9
Axisymmetric/	0 (Baseline)	1.0	——	——
Mach 10	800 W	0.760	11.0	0.9
	800 W	0.730	12.5	1.15
	800 W	0.460	25.0	1.55
	800 W	0.300	33.0	2.00
	800 W	0.310	32.5	2.55
Axisymmetric/	0 (Baseline)	1.0	——	——
Mach 6.5	10 W	0.956	48.24	0.9
	50 W	0.94	13.06	0.9
	100 W	0.852	16.06	0.9
	200 W	0.686	17.06	0.9
Two dimensional/	0 (Baseline)	1.0	——	——
Mach 2.5	1 kW/m	0.7	12.34	0.9

upstream of the blunt body. The parameter x/h provides the axial location of the energized region normalized in terms of body diameters (for the axisymmetric cases) or in terms of body widths (for the two-dimensional cases). The first series of cases listed in Table 1 is for two-dimensional flow about the blunt body (wing slab) at Mach 6.5; the first case in this series corresponds to the reference blunt body (no energy deposition). For the rest of the cases in this series, the energy-deposition location is fixed at $x/h = 0.9$, and energy-deposition rates are varied from 2 to 30 kW/m. Note that for all two-dimensional cases the power input is given per unit width of the wing slab.

The next series of cases listed in Table 1 is for flow about an axisymmetric blunt body with a hemispherical nose at Mach 10. The first of the six cases in this series is the reference blunt-body flowfield (no energy deposition). In this particular series, the energy-deposition rate is fixed at 800 W while the axial location of the energy deposition region is varied from $x/h = 0.9$ to $x/h = 2.55$. The third series of cases corresponds to Mach 6.5 flow over an axisymmetric blunt body. Again, the first case is the reference (no-energy) case. The energy-deposition location is fixed in this series, and energy deposition rates are varied as shown in Table 1. The final two cases are for Mach 2.5 flow (two-dimensional blunt body) for no power input and 1-kW/m power input, respectively.

VI. Discussion of Results

Figure 3 shows normalized drag R vs the energy deposition rate in kilowatts per meter width for the Mach 6.5, two-dimensional blunt-body series of cases (all with a fixed energy-deposition location). For the maximum energy addition rate investigated (30 kW/m), the drag drops to 50% of the baseline drag. Figure 3 indicates an asymptotic approach to a drag reduction of about 45% at high energy addition rate levels; however, these data are for a fixed (unoptimized) and relatively near-field energy-deposition location. Shown in Fig. 4 is the power effectiveness S for the same series of cases. Very high effectiveness is seen to occur for very small energy-deposition rates; however, correspondingly small drag reductions (see Fig. 3) are obtained for such cases as well. The power effectiveness values are nevertheless quite high for all power-deposition levels; for instance, for the 20-kW/m case, the power effectiveness is almost 15, i.e., 15 units of required thrust power are saved at the cost of a single unit of power input into the upstream flow. Furthermore, even if the overall efficiency of the deposition technique is as low as 20%, there is still a net 3:1 power savings. Also, recall that no attempt has been made to optimize energy-deposition location in this series of cases.

Figure 5 shows the normalized drag R vs x/h for a constant upstream power addition of 800 kW for the axisymmetric Mach 10 series of cases listed in Table 1. There is a steep drop in drag as x/h increases from 1 to 2, with an overall minimum in R occurring at $x/h = 2$. This minimum drag corresponds to 30% of the baseline drag. It is followed by relatively flat drag values for x/h between 2 and 2.5 upstream of the body. (It is believed that eventually the drag curve would swing more or less sharply back toward the reference no-energy value as separation distances were further increased, although this is not verified in this study.) For this series of cases, Fig. 6 demonstrates that the power effectiveness peaks at the same location as the drag is minimized, i.e., drag is minimized and power effectiveness is maximized when the energy is deposited two body

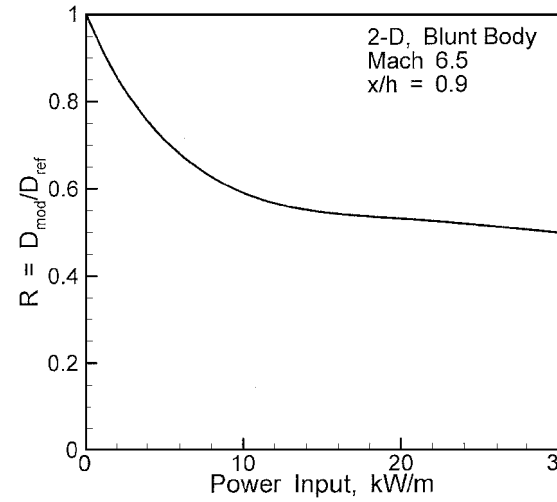

Fig. 3 Normalized drag R vs focused power input.

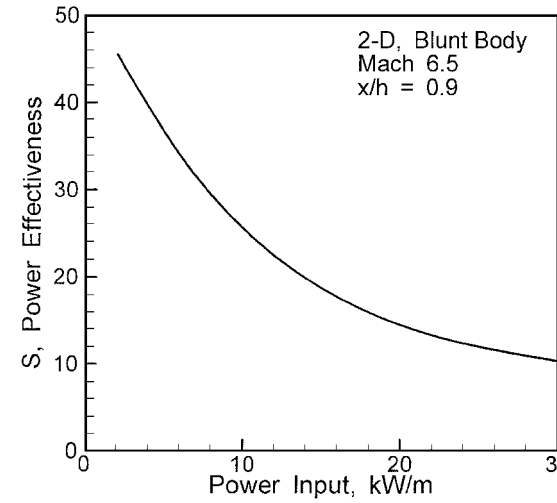

Fig. 4 Power effectiveness S vs focused power input.

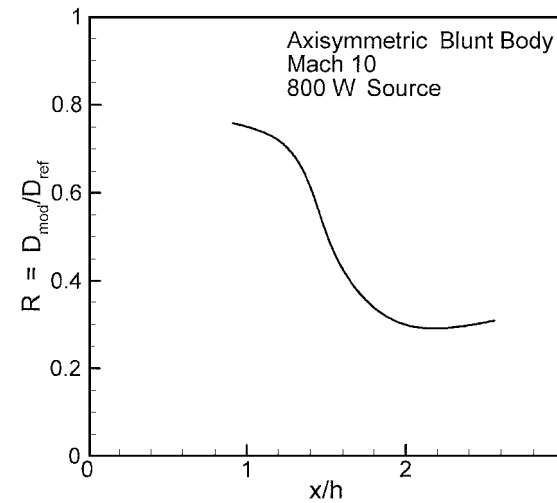

Fig. 5 Normalized drag R vs axial location of 800-W power source.

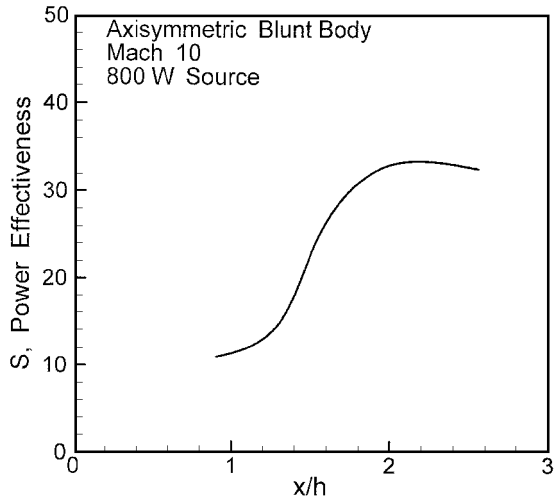

Fig. 6 Power effectiveness S vs axial location of 800-W power source.

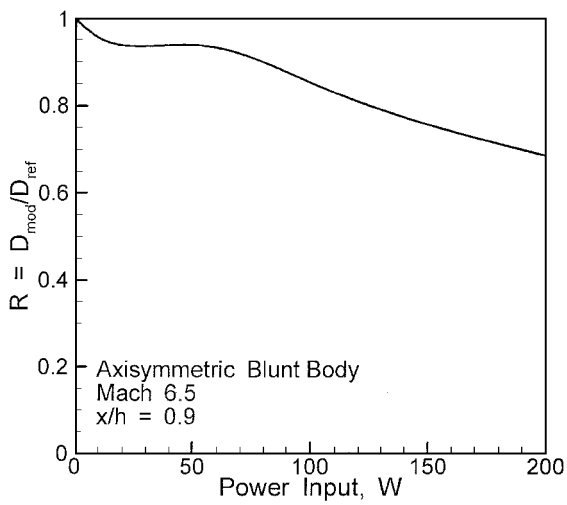

Fig. 7 Normalized drag R vs focused power input.

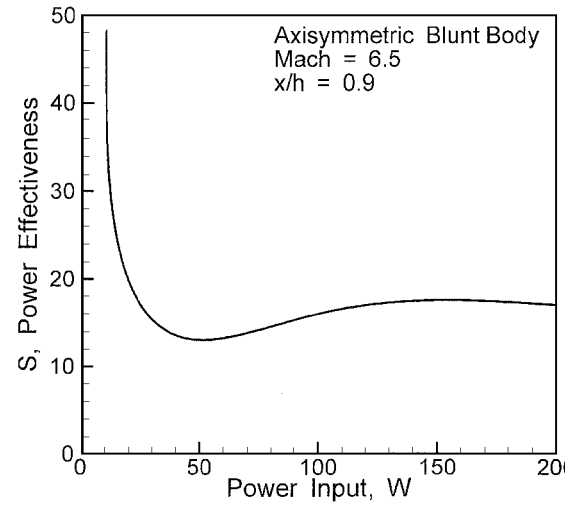

Fig. 8 Power effectiveness S vs focused power input.

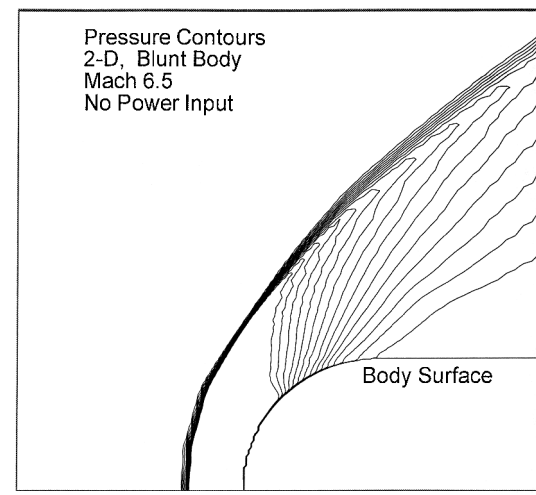

Fig. 9 Pressure contours: Mach 6.5, two-dimensional blunt body; zero power input (baseline).

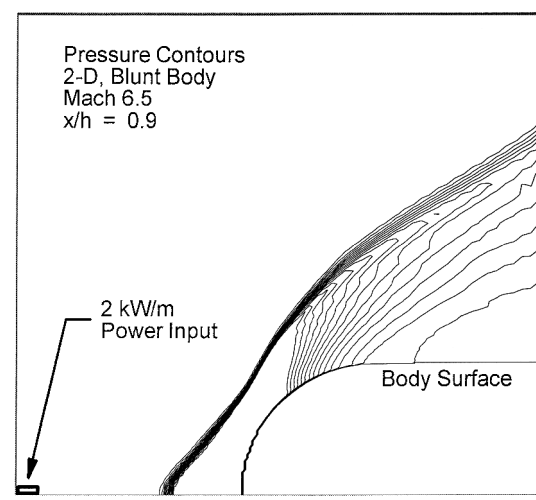

Fig. 10 Pressure contours: Mach 6.5, two-dimensional blunt body; 2-kW/m power input, $x/h = 0.9$.

diameters upstream of the blunt-body nose. This also agrees with Eq. (2) for constant func $\dot{Q}$. The value of S for this case is 33, in other words 33 units of thrust power saved at the cost of 1 unit of power deposited into the upstream flow and corresponding to 30% of the baseline drag. Again, even if the overall efficiency of the energy-deposition technique (including transmission, absorption, etc.) was 20%, there is approximately a net 7:1 power saving for the vehicle. Note that for this series of cases no attempt has been made to optimize the energy-deposition rate magnitude.

Figures 7 and 8 are similar to Figs. 3 and 4 except that they correspond to the Mach 6.5 axisymmetric blunt-body (instead of Mach 6.5, two-dimensional blunt-body) series of cases with variable energy level and fixed energization location. Although drag reduction in Fig. 7 is not as large as in Fig. 3, it must be emphasized that both optimization of energy-deposition location and power levels are critical for effective drag reduction, as made clear in the discussion of Figs. 3–6. Significantly, no case analyzed in this investigation had a power effectiveness of less than 10.

To illustrate the modification of the flowfield due to the upstream energy addition and to clarify the reasons for the drag reduction, pressure contours for individual cases from the Mach 6.5, two-dimensional blunt-body series are shown in Figs. 9–13. Figures 9–13 present results for a range of $\dot{Q}$ between zero (baseline) and 30 kW/m. In all cases, the energy-deposition region is located at the extreme lower left-hand corner of the flowfield ($x/h = 0.9$). Figure 9 represents the baseline (no-energy) blunt-body flowfield; shock standoff distance and shock shape agree reasonably well with the empirical correlations of Billig.[11] When 2-kW/m power is added (deposited) in the upstream stagnation streamtube, as indicated in Fig. 10, there is an increase in the normal shock standoff distance and a correspondingly more rapid evolution of this normal shock into an oblique shock away from the centerline, along with attendant flow relieving in the downstream (postshock) zone. This change in the flowfield characteristics is believed to be due primarily to the thermal effect of the heating of the flow and the subsequent reduction in stagnation streamline Mach number between the energized region and the body. Although not shown in

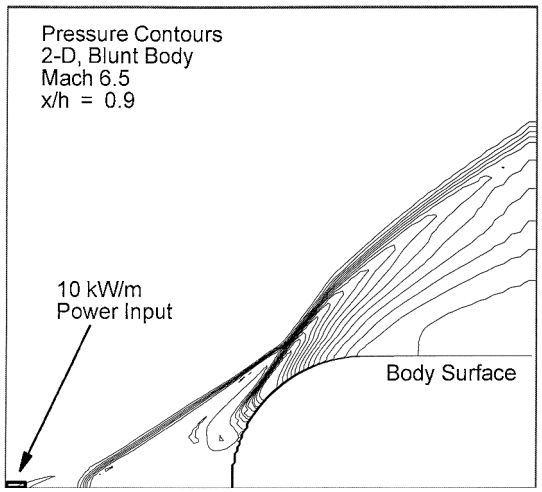

Fig. 11 Pressure contours: Mach 6.5, two-dimensional blunt body; 10-kW/m power input, $x/h = 0.9$.

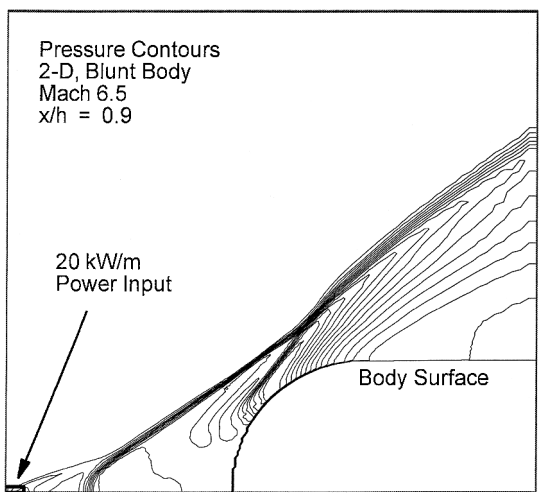

Fig. 12 Pressure contours: Mach 6.5, two-dimensional blunt body; 20-kW/m power input, $x/h = 0.9$.

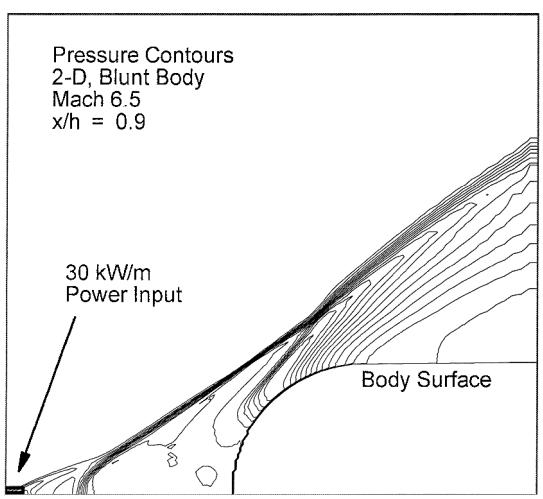

Fig. 13 Pressure contours: Mach 6.5, two-dimensional blunt body; 30-kW/m power input, $x/h = 0.9$.

Fig. 9, the details of the energized region itself are characterized by discernible flow turning due to the pressurization of the region with weak oblique waves forming from the turned (energized) flow. In this sense, the thermally heated region acts somewhat like a small stationary low-angle wedge fixed in the flow upstream of the body. The weak oblique compression waves associated with the energy deposition can be seen in Fig. 11 (for 10-kW/m power input). In this case, the normal shock weakens yet further, is pulled farther from the body, and essentially becomes a strong oblique wave downstream of the energy-deposition region except where it intersects the stagnation streamtube itself. A relatively large triangular stagnation region forms, with its apex located just downstream of the normal shock at the centerline of the flow. The bulk outer flow is turned; however, the external flow still impinges upon the (upper) forward surface of the cylindrical nose, and hence, a secondary shock forms just off the body. This secondary shock then joins the primary oblique shock near the body shoulder. (This effect can also be clearly seen by viewing the velocity vectors for the 20-kW/m case shown in Fig 2b.) The secondary shock appears to weaken as the power input increases from 20 to 30 kW/m, as shown in Figs. 12 and 13. In general, as power input increases from 2 to 30 kW/m, the subsonic region increases in size, the flow turning associated with both the energy-deposition magnitude and the main oblique shock increases, and at higher power input values the secondary shock progressively weakens. This flowfield structure and streamline turning are due to an effective increase in the aerodynamic fineness ratio of the body. It is readily projected from these observations that increasing x/h (distance between the energized region and the blunt-body nose) may in fact allow similar flowfield modifications for smaller input power levels. In any event, reduction of the pressure on the body surface as the secondary shock weakens and upstream flow turning increases generates a significant and progressive reduction in wave drag on the blunt body (as deposited energy levels are increased).

It is also instructive to examine static pressure on the centerline (stagnation) streamtube and along the blunt-body surface for representative cases. Figure 14 shows the pressure trace for three cases for Mach 6.5 flow around a two-dimensional blunt body. These cases (indicated in Fig. 14) correspond to 1) reference blunt body (no energy addition), 2) 20-kW/m power input at 0.9 body widths upstream, and 3) a small wedge flying ahead of the blunt body as described earlier and detailed in Fig. 1. The surface of the blunt body is labeled in Fig. 14. Variations in pressure behind the normal shock are due to small-scale, time-dependent vortical motion in the subsonic region upstream of the nose. The reference case shows the expected pressurization downstream of the strong normal shock and subsequent pressure relief along the body surface. The upstream wedge case exhibits a sharp rise in pressure due to the presence of the wedge shock followed by the relatively flat pressure downstream of the wedge to the nose of the blunt body. This constant pressure region is associated with the wedge-shaped stagnation zone that lies between the wedge and the blunt body. The outer flow, although turned by the small wedge, still impinges on the upper forward surface of the body nose, as is evident by the secondary rise in pressure. The flow then turns back over the contour of the blunt body.

The pressure trace for the 20-kW/m case shows a relatively small pressure rise associated with the energized region, which is followed by relaxation downstream until the intermediate normal-oblique shock is encountered. The pressure trace is then relatively constant

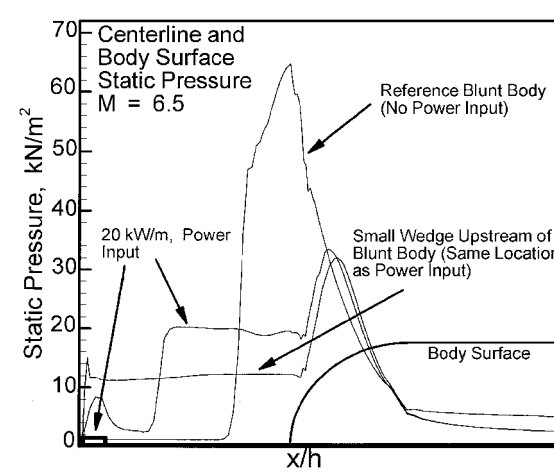

Fig. 14 Static pressure trace along centerline (upstream of body) and along body surface; Mach 6.5, two-dimensional blunt body for three cases: reference blunt body, small wedge at $x/h = 0.9$, and 20-kW/m power input at $x/h = 0.9$.

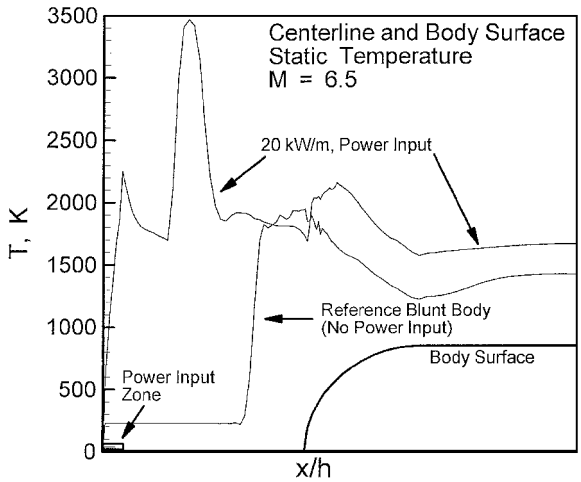

Fig. 15 Static temperature trace along centerline (upstream of body) and along body surface; Mach 6.5, two-dimensional blunt body for two cases: reference blunt body and 20-kW/m power input at $x/h = 0.9$.

along the centerline and over the body surface until the secondary rise associated with the secondary shock is encountered. The similarity between the pressure traces on the body surface leads to approximately equivalent drags for the upstream wedge and the 20-kW/m cases.

Finally, to study the effect of the energy addition on the fluid temperature adjacent to the body (and ultimately the heat transfer to the body), Fig. 15 shows temperature along the centerline (stagnation) streamtube and just above the blunt-body surface for both the reference no-energy case and the 20-kW/m case for Mach 6.5, two-dimensional flow. The characteristics of the temperature trace for the reference case are similar to the corresponding pressure trace shown in Fig. 14. For the energy-deposition case, the normal/oblique shock temperature rise is evident; however, this higher-temperature (energized) region is quite small and exists only on the centerline streamtube. In the subsonic (low-velocity) region behind the shock, there is a great deal of heat conduction to the cooler, higher-velocity regions adjacent to the centerline region. This results in the sharp drop in temperature from about 3500 to 1800 K within the upstream region. The temperature along the body surface then follows the same trend as the temperature along the reference blunt body, although it remains about 250 degrees higher due to the upstream energy addition. There is, however, also a small rise in temperature from about 1750 to 2250 K associated with the secondary shock on the shoulder of the body. Although there is a small increase in surface temperature due to the upstream energization for this case, recall that there is a corresponding and significant (50%) decrease in wave drag.

VII. Conclusions

This paper provides a parametric study and analysis of the use of tightly focused energy deposition within a flowfield for the modification and attenuation of shock wave structure associated with supersonic and hypersonic flow about blunt bodies. The computational and physical methodologies used in this investigation are reviewed in detail. Similarity of the flowfields for a representative energy-deposition case and an upstream physical spike is shown and discussed qualitatively. Performance parameters for use in characterizing and evaluating the feasibility of the energy-deposition technique are developed and are applied to a large matrix of energy-deposition cases including reference (zero-energy) cases. The matrix of cases span Mach numbers from 2.5 to 10 for both axisymmetric and two-dimensional blunt-body configurations. Energy-deposition rate levels and energy-deposition rate locations are parametrically varied within this matrix. The fluid dynamics and thermodynamics of the energy deposition and attendant reductions in wave drag are studied by examining flowfields and contrasting wall pressure and temperature traces for representative cases.

The correct implementation of tightly focused energy deposition upstream of a blunt body in high-speed flow is shown to result in dramatic decreases in wave drag. Drag values on the order of 30–50% of the baseline (no-energy) cases are readily obtained without simultaneous optimization of both energy location and energy level. These drag reductions are obtained with power requirements as low as 3% of the thrust power (necessary to cruise) saved by the method; i.e., the technique can withstand very large inefficiencies throughout the energy-deposition system. Extremely promising results have been obtained for flight Mach numbers of 6.5 and 10, with more limited information obtained at a flight Mach number of 2.5.

The mechanism of drag reduction within the flows examined is purely a thermodynamic and fluid dynamic phenomenon (although the mechanism is quite complex). The immediate effect of focused upstream energy addition is to heat, pressurize, and slow the energized fluid; if sufficient energy is provided, weak adjacent compression waves are observed forming around the energized region. However, it is the strong coupling between the energized region and the (downstream) blunt-body nose that dominates the change in flow structure; the blunt-body normal shock weakens and moves far upstream toward the energized region, thus resulting in very rapid lateral transition of this shock into an oblique wave. This oblique shock is coupled with the weaker compression waves emanating from the energized region. The flow between this primary shock structure and the blunt body is characterized by a wedge-shaped stagnation (low-speed) region, similar to that observed downstream of a small (physical) wedge. Depending on energy amount and location, outer flow turning may be sufficient to envelope the body such that any secondary shock structure along the top forward body surface is reduced in strength or even eliminated. As a result, the pressure drag on the body can drop dramatically from that of a blunt body with no power deposition in the flow. However, there is increased heating of the body surface due to the upstream energization; for the cases examined in this investigation, this increase is moderate. The magnitude of the drag reduction and power-based effectiveness ratios demonstrated here strongly mandate further investigation.

Appendix: Grid and Temporal Convergence for Modeling of Energy Deposition

This section provides a summary of grid and temporal convergence results for a representative case (Mach 6.5, two-dimensional, blunt body) with high energy deposition focused upstream. The baseline grid used in the preceding parametric study is composed of 105 (axial) and 101 (vertical) nodes. To assess the effect of grid refinement on both wave drag and details of the flowfield, a solution was obtained with 209 (axial) nodes and 201 (vertical) nodes, representing a doubling of refinement in both coordinate directions. An identical (high) energy-deposition rate is used in both cases. Figures A1 and A2 present pressure contours with identical scales for the baseline grid and for the refined grid, respectively. The contours have virtually identical spatial flow patterns; there is no significant difference in the flowfield due to grid refinement. Figure A3

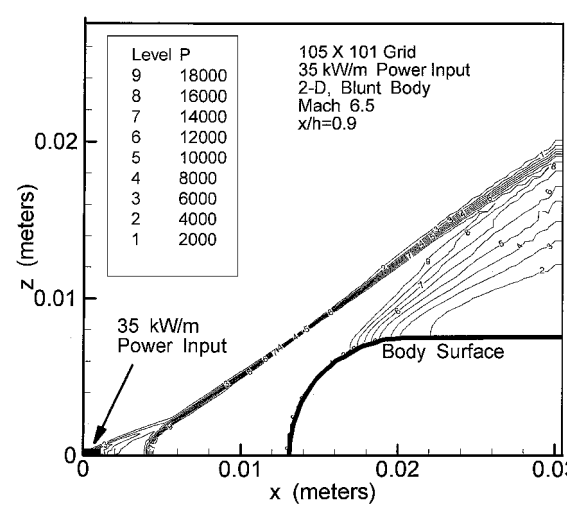

Fig. A1 Pressure contours for two-dimensional blunt body, Mach 6.5, upstream energization at $x/h = 0.9$ (upstream of body nose); baseline grid (105 × 101).

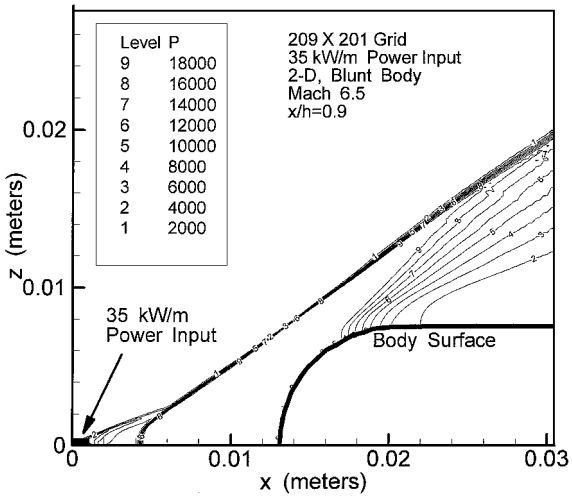

Fig. A2 Pressure contours for two-dimensional blunt body, Mach 6.5, upstream energization at $x/h = 0.9$ (upstream of body nose); refined grid (209 × 201).

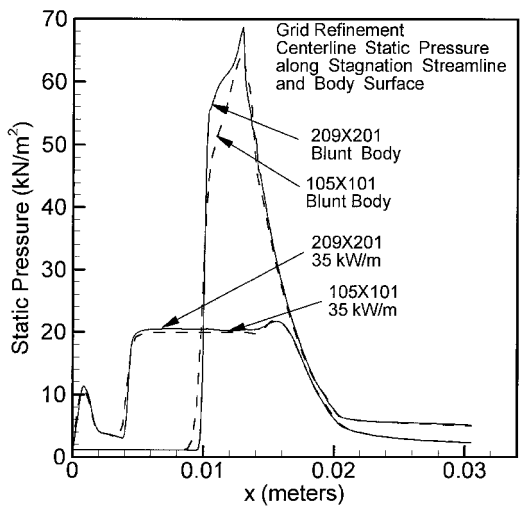

Fig. A3 Static pressure trace along centerline (upstream of body) and along body surface; Mach 6.5, two-dimensional blunt body, with and without energy deposition for refined and baseline grids.

shows a detailed plot of static pressure along the stagnation streamline upstream of the blunt body and along the body surface. Four cases are shown: 1) fine grid with high energy deposition, 2) baseline grid with high energy deposition, 3) fine grid with no energy deposition (reference blunt body), and 4) baseline grid with no energy deposition (reference blunt body). Again, the reference blunt-body cases and the energy-deposition cases demonstrate a very high degree of grid convergence; there is no significant difference between the results obtained with the refined and with the baseline grid. The integrated wave drag levels for the refined and baseline grid cases differ approximately 1%.

Figure A4 provides a time history of wave drag for the baseline grid with high energy deposition. The wave drag quickly reaches its asymptotic value. Recall that wave drag is the parameter of interest in this study. No instabilities are evident in the flow due to the energy deposition.

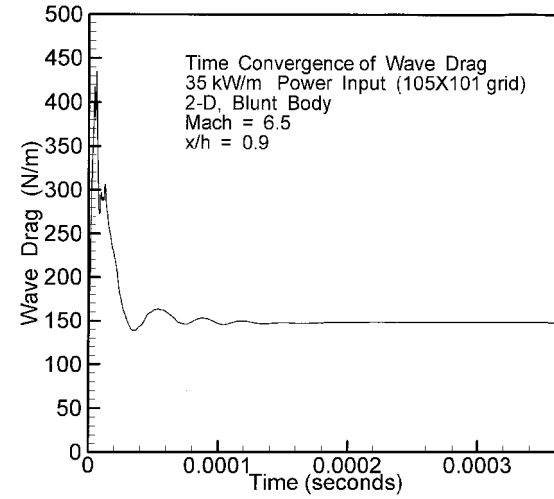

Fig. A4 Time convergence history for wave drag; Mach 6.5, two-dimensional blunt body, upstream energization at $x/h = 0.9$.

Acknowledgments

This work was partially supported by NASA Grant NAG-1189 from the HYPER-X Program Office, C. R. McClinton, Technical Monitor. The authors would like to gratefully acknowledge both Charles McClinton and Dennis Bushnell from NASA Langley Research Center, the former for his support and patience and the latter for his encouragement and interest regarding this and other topics.

References

[1]Hutt, C. R., and Howe, A. J., "Forward Facing Spike Effects of Bodies of Different Cross Sections in Supersonic Flow," *Aeronautical Journal of the Royal Aeronautical Society*, Vol. 93, No. 926, 1989, pp. 229–234.

[2]Bushnell, D. M., "Supersonic Aircraft Drag Reduction," AIAA Paper 90-1596, June 1990.

[3]Miller, D. S., and Carlson, H. W., "A Study of the Application of Heat or Force Field to the Sonic-Boom-Minimization Problem," NASA TN-D-5582, Dec. 1969.

[4]Miller, D. S., and Carlson, H. W., "On the Application of Heat or Force Field to the Sonic-Boom-Minimization Problem," AIAA Paper 70-903, July 1970.

[5]Batdorf, S. B., "On Alleviation of the Sonic Boom by Thermal Means," AIAA Paper 70-1323, Oct. 1970.

[6]Toro, P. G. P., Myrabo, L. N., and Nagamatsu, H. T., "Pressure Investigation of the Hypersonic 'Directed-Energy Air Spike' Inlet at Mach Number 10 up to 70 kW," AIAA Paper 98-0991, Jan. 1998.

[7]Marconi, F., "An Investigation of Tailored Upstream Heating for Sonic Boom and Drag Reduction," AIAA Paper 98-0333, Jan. 1998.

[8]Mishin, G. I., "Experimental Investigation of the Flight of a Sphere in Weakly Ionized Air," AIAA Paper 97-2298, June 1997.

[9]Vlasov, V. V., Grudnitskii, B. G., and Rygalin, V. N., "Gas Dynamics with Local Energy Release in Subsonic and Supersonic Flow," *Fluid Dynamics*, Vol. 30, No. 2, 1995, pp. 275–280.

[10]Drummond, J. P., Rogers, R. C., and Hussaini, M. Y., "A Detailed Numerical Model of a Supersonic Reacting Mixing Layer," AIAA Paper 86-1427, June 1986.

[11]Billig, F. S., "Shock-Wave Shapes Around Spherical- and Cylindrical-Nosed Bodies," *Journal of Spacecraft and Rockets*, Vol. 4, No. 6, 1967, pp. 822, 823.

A. Plotkin
Associate Editor